Appendix A
Optimizing Total Power Consumption by Defining Total Noise and Total Nonlinearity

Using (2.6) and considering third order nonlinearity as the only dominant order of nonlinearity, $V^2_{int,tot}$ can be described as a function of $V^2_{IP3i,tot}$:

$$\bar{V}^2_{ni,tot} = \frac{NPD - kTB}{B(R_s + R_{in})^2} \times 4R_sR^2_{in} - \frac{V^6_{interferer}}{BV^4_{IP3i,tot}} \tag{A.1}$$

Replacing the result in (2.31), we have:

$$P_{tot} = \frac{BV^6_{IP3i,tot}}{\frac{NPD-kTB}{(R_s+R_{in})^2} \times 4R_sR^2_{in} \times V^4_{IP3i,tot} - V^6_{interferer}} \times \left(\sum_{m=1}^{N} \sqrt[3]{P_{Cm}}\right)^3 \tag{A.2}$$

Taking the derivative of P_{tot} with respect to $V^2_{IP3i,tot}$, we have:

$$\frac{\partial P_{tot}}{\partial\left(V^2_{IP3i,tot}\right)} = \frac{BV^4_{IP3i,tot}\left(\frac{NPD-kTB}{(R_s+R_{in})^2} \times 4R_sR^2_{in} \times V^4_{IP3i,tot} - 3V^6_{interferer}\right)}{\left(\frac{NPD-kTB}{(R_s+R_{in})^2} \times 4R_sR^2_{in} \times V^4_{IP3i,tot} - V^6_{interferer}\right)^2} \times \left(\sum_{m=1}^{N} \sqrt[3]{P_{Cm}}\right)^3 \tag{A.3}$$

Setting (A.3) to zero, we have:

$$V^4_{IP3i,tot} = \frac{3V^6_{interferer}}{\frac{NPD-kTB}{(R_s+R_{in})^2} \times 4R_sR^2_{in}} \tag{A.4}$$

Using (2.3) and (2.5), $V_{IMD3i,tot}$ can be obtained:

$$V^2_{IMD3i,tot} = \frac{NPD - kTB}{(R_s + R_{in})^2} \times 4R_sR^2_{in} \times \frac{1}{3} = \frac{B\bar{V}^2_{ni,tot}}{2} \tag{A.5}$$

which results in (2.21).

P. Sakian et al., *RF-Frontend Design for Process-Variation-Tolerant Receivers*, Analog Circuits and Signal Processing, DOI 10.1007/978-1-4614-2122-1,

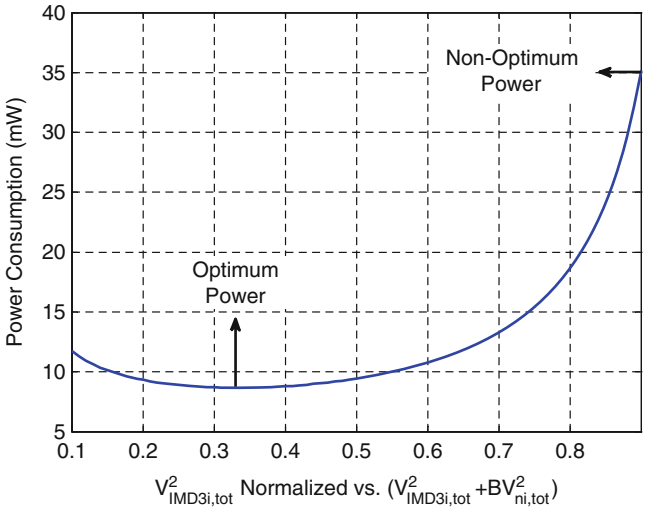

Fig. A.1 Power consumption given by the optimum-power design method as a function of $V^2_{IMD3i,tot}$ for a constant NPD.

Figure A.1 shows the power consumption of a receiver (described in detail in Sect. 2.8) as a function of $V^2_{IMD3i,tot}$. In other words, $V^2_{IMD3i,tot}$ and $BV^2_{ni,tot}$ are varied in a way that their sum remains constant so that NPD remains unchanged. For each value of $V^2_{IMD3i,tot}$ and $BV^2_{ni,tot}$ the power consumption is calculated according to optimum-power method using (2.31). Based on Fig. A.1, minimum power consumption is achieved when $V^2_{IMD3i,tot}$ constitutes one third of ($V^2_{IMD3i,tot}$ + $BV^2_{ni,tot}$) which is in agreement with (2.21). In the extremes the power consumption can be much higher, for example when $V^2_{IMD3i,tot}$ comprises 90% of ($V^2_{IMD3i,tot}$ + $BV^2_{ni,tot}$), the blocks need to be extremely low-noise and the power consumption can be more than four times higher than the minimum.

Glossary

Symbol	Description	Unit
A	Amplitude of the sinusoidal output of the VCO	V
A_v	Voltage conversion gain of the mixer	
$A_{vn,k}$	Voltage gain of the k^{th} stage at the signal band including the loading effects	
$A_{vn,k,image}$	Voltage gain of the k^{th} stage at the image band including the loading effects	
$A_{vn,tot}$	Voltage gain of the whole receiver at the signal band	
$A_{vn,tot,image}$	Voltage gain of the whole receiver at the image band	
B	Effective noise bandwidth	Hz
B_{CS}	B element of the T matrix of a transistor in common-source configuration	Ω
B_x	B element of the T matrix of a transistor in source-follower configuration	Ω
B_{sig}	Signal bandwidth	Hz
C_{max}	Maximum capacitance of the LC-tank	F
C_{min}	Minimum capacitance of the LC-tank	F
$C_{ImA,k}$	Ratio between the square of voltage gain at the image band to the square of voltage gain at the signal band calculated for the k^{th} stage	
$C_{ImN,k}$	Ratio between the square of the noise voltage at the image band to the square of the noise voltage at the signal band calculated for the k^{th} stage	
$C_{Distortion,q}(k)$	Contribution of the k^{th} stage to the total q^{th} order intermodulation distortion	V^2
c_{gd}	Gate-drain capacitance	F
c_{gs}	Gate-source capacitance	F
C_L	Load capacitance	F
C_{L1}	The capacitance seen from the positive node of the differential output	F
C_{L2}	The capacitance seen from the negative node of the differential output	F
$C_{Noise}(k)$	Contribution of the k^{th} stage to the total noise	V^2
C_{ox}	Oxide capacitance of a MOS transistor	F/m^2

(continued)

Symbol	Description	Unit
C_P	The equivalent capacitance after performing series-to-parallel conversion on the tank capacitance	F
C_s	Capacitances at the common source of the switching pair of the mixer	F
D_{CS}	D element of the T matrix of a transistor in common-source configuration	
D_x	D element of the T matrix of a transistor in source-follower configuration	
F	An empirical parameter called effective noise figure by Leeson	
G_1	First order Volterra kernel from RF current to the gate-source voltage of the mixer	Ω
G_2	Second order Volterra kernel from RF current to the gate-source voltage of the mixer	V/A^2
G_3	Second order Volterra kernel from RF current to the gate-source voltage of the mixer	V/A^3
g_{d0}	Transistor channel conductance when the drain-source voltage is zero	1/Ω
g_m	First-order transconductance of the transistor	1/Ω
g_{m2}	Second-order transconductance of the transistor	A/V^2
g_{m3}	Third-order transconductance of the transistor	A/V^3
G_C	Power conversion gain of the mixer	
G_T	Transducer power gain	
g_s	Inverse of R_S	1/Ω
I_{DS}	Drain-source biasing current of the transistor	A
$I_{imd2,1}$	IMD2 current in the first branch of the differential output of the mixer	A
$I_{imd2,2}$	IMD2 current in the second branch of the differential output of the mixer	A
I_{imd2CM}	Common-mode output IMD2 current of the mixer	A
$I_{imd2Diff}$	Differential-mode output IMD2 current of the mixer	A
I_{Out}	Differential output current of the switching pair of the mixer	A
I_{Out3}	Third-order intermodulation content in the differential output current of the switching pair of the mixer	A
I_{pk}	The amplitude of the sinusoidal current	A
I_{RF}	RF current flowing into the switching pair of the mixer	A
IP3	Third order input intercept point	dBm
k	Boltzmann constant $= 1.38 \times 10^{-23}$	J/K
k_c	Coupling factor between two inductors	
L_D	Drain inductance	H
L_G	Gate inductance	H
L_P	The equivalent inductance after performing series-to-parallel conversion on the tank inductance	H
L_S	Source inductance (connected to the source of the transistor)	H
M	Mutual inductance	H
MDS	Minimum detectable signal of a receiver (also known as sensitivity)	dBm
n	Turn ratio of a transformer	
N	Number of stages in the receiver	

(continued)

Symbol	Description	Unit
$N_{Antenna}$	Available noise power coming from the antenna	W
$N_{i,tot}$	The total available noise power due to the receiver referred to its input	W
NF_{tot}	Noise factor of the whole receiver	dB
NPD	Noise plus distortion of a receiver referred to its input	W
P	Power consumption of a stage	W
P_{Ck}	Power coefficient of the k^{th} stage: a proportionality constant relating the power consumption to the noise and linearity performance	W
$P_{IMDqi,tot}$	Equivalent input-referred available power of in-band q^{th} order intermodulation distortion due to an out-of-band interferer	W
P_S	Average power dissipated in the resistive part of the tank	W
P_{tot}	Power consumption of the whole receiver	W
Q	Effective quality factor of the tank	
Q_C	Quality factor of the tank capacitance	
Q_L	Quality factor of the tank inductance	
R_{CP}	Equivalent parallel resistance of the tank capacitance	Ω
R_{CS}	Series resistance of the tank capacitance	Ω
R_G	Gate resistance	Ω
R_{in}	Real part of the input impedance	Ω
R_L	Load resistance	Ω
R_{LP}	Equivalent parallel resistance of the tank inductance	Ω
R_{LS}	Series resistance of the tank inductance	Ω
r_o	Output resistance of the transistor	Ω
R_{out1}	The real part of the impedance seen from the positive node of the differential output	Ω
R_{out2}	The real part of the impedance seen from the negative node of the differential output	Ω
R_S	Source resistance	Ω
$S_x^{F(x)}$	Normalized single point sensitivity of F(x) to the variable x	
SNDR	Signal to noise-plus-distortion ratio	dB
T	Absolute temperature	K
T_0	Reference temperature for noise figure definition: 290°K	K
TR	Tuning range of a VCO	
U	Mason invariant: the gain of a linear two-port after unilateraliztion by embedding in a linear lossless reciprocal four-port	
V_{gs}	Gate-source voltage	V
$V_{imd2out}$	Differential output IMD2 voltage of the mixer	V
$V_{IMDqi,k}$	Equivalent input-referred voltage of the q^{th} order intermodulation distortion of the k^{th} stage of the receiver	V
$V_{IMDqi,tot}$	Equivalent input-referred voltage of the q^{th} order intermodulation distortion of the whole receiver	V
$V_{interferer}$	Voltage of worst-case out-of-band interferer signal at the input of the receiver	V
$V_{IPqi,k}$	Voltage of q^{th} order input intercept point of the k^{th} stage of the receiver	V
$V_{IPqi,tot}$	Voltage of q^{th} order input intercept point of the whole receiver	V
V_{LO}	Local oscillator voltage connected to the LO port of the mixer	V

(continued)

Symbol	Description	Unit
$V_{ni,k}$	Equivalent input-referred noise voltage of the k^{th} stage of the receiver	V/√Hz
$V_{ni,tot}$	Equivalent input-referred noise voltage of the whole receiver	V/√Hz
$V_{nout,k}$	Noise voltage due to the k^{th} stage at the output of the stage and at the signal band	V/√Hz
$V_{nout,k,image}$	Noise voltage due to the k^{th} stage at the output of the stage and at the image band	V/√Hz
$V_{nout,Rs}$	Noise at the output of the mixer due to the source resistance	V/√Hz
$V_{nout,RL}$	Noise at the output of the mixer due to the load resistance	V/√Hz
$V_{nout,sw}$	Noise at the output of the mixer due to the switching pair	V/√Hz
$V_{nout,tot}$	Noise voltage due to the whole receiver at the output of the receiver and at the signal band	V/√Hz
$V_{nout,k,image}$	Noise voltage due to the whole receiver at the output of the receiver and at the image band	V/√Hz
V_{off}	Equivalent voltage offset representing the mismatch between the transistors in a differential pair	V
V_{out-}	Voltage of the negative node of the differential output	V
V_{out+}	Voltage of the positive node of the differential output	V
V_{RF}	RF voltage connected to the RF port of the mixer	V
V_T	Threshold voltage of a MOS transistor	V
W	Transistor width	m
X_{in}	Imaginary part of the input impedance	Ω
Z	Impedance matrix of a two-port	Ω
Z_{in}	Input impedance	Ω
Z_{L1}	The impedance seen from the positive node of the differential output	Ω
Z_{L2}	The impedance seen from the negative node of the differential output	Ω
Z_{src}	Source impedance	Ω
α_k	Contribution factor: the ratio between the noise (or distortion) contribution of the k^{th} stage to that of its following stage	
β	Proportionality constant between the current in an MOS transistor and the square of the difference between gate-source voltage and threshold voltage	A/V^2
γ	Transistor channel noise coefficient	
ΔNPD	Variations of the noise plus distortion of a receiver referred to its input	W
$\Delta V_{IPqi,k}$	Variations of the voltage of q^{th} order input intercept point of the k^{th} stage of the receiver	V
$\Delta V_{ni,k}$	Variations of equivalent input-referred noise voltage of the k^{th} stage of the receiver	V/√Hz
ΔV_T	Absolute mismatch between the threshold voltage of the transistors in a differential pair	V
ΔZ_{in}	Variations of input impedance	Ω
δZ_L	Relative mismatch in the differential load impedance	
Δβ	Absolute mismatch between the β of the transistors in a differential pair	A/V^2
Δθ		1/V

(continued)

Symbol	Description	Unit
	Absolute mismatch between the θ of the transistors in a differential pair	
$\Delta\omega$	Offset from the oscillation angular frequency of the VCO	rad/s
$\Delta\omega_{1/f^3}$	Angular frequency of the corner between $1/f^3$ and $1/f^2$ regions	rad/s
θ	A fitting factor taking into account the short channel effects of MOS transistors	1/V
μ_n	The mobility of an NMOS transistor	$m^2/V/s$
τ	Time constant at the common-source node of the switching pair of the mixer	s
$\Phi(t)$	Phase of the sinusoidal output of a VCO	rad
$\varphi_{IMDqi,k}$	The phase of the equivalent input-referred voltage of the q^{th} order intermodulation distortion of the k^{th} stage	rad
$\varphi_{IMDqi,tot}$	The phase of the equivalent input-referred voltage of the q^{th} order intermodulation distortion of the whole receiver	rad
$\varphi_{IPqi,k}$	Phase of the voltage of the q^{th} order input intercept point of the k^{th} stage	V
$\varphi_{IPqi,tot}$	Phase of the voltage of the q^{th} order input intercept point of the whole receiver	V
$\varphi_{vn,k}$	The phase of the voltage gain of the k^{th} stage at the signal band including the loading effects	rad
$\varphi_{vn,tot}$	The phase of the voltage gain of the whole receiver at the signal band	rad
ω	Angular frequency	rad/s
ω_0	Oscillation angular frequency of a VCO	rad/s
ω_1	Angular frequency of the first tone in a multi-tone signal	rad/s
ω_2	Angular frequency of the second tone in a multi-tone signal	rad/s
ω_3	Angular frequency of the third tone in a multi-tone signal	rad/s
ω_{center}	Center (the middle of the maximum and minimum) angular frequency of oscillation of a VCO	rad/s
ω_{IF}	IF Angular frequency	rad/s
ω_{LO}	LO Angular frequency	rad/s
ω_{max}	Maximum angular frequency of oscillation of a VCO	rad/s
ω_{min}	Minimum angular frequency of oscillation of a VCO	rad/s

Bibliography

1. Ramakrishnan H, Shedabale S, Russell G, Yakovlev A (2008) Analysing the effect of process variation to reduce parametric yield loss. IEEE international conference on integrated circuit design and technology, June 2008, pp 171–176
2. Springer SK, Lee S, Lu N, Nowak EJ, Plouchart J-O, Watts JS, Williams RQ, Zamdmer N (2006) Modeling of variation in submicrometer CMOS ULSI technologies. IEEE Trans Electron Dev 53(9):2168–2178
3. Sery G, Borkar S, De V (2002) Life is CMOS: why chase the life after? Proceedings of 39th design automation conference, pp 78–83
4. Karnik T, Borkar S, De V (2002) Sub-90 nm technologies-challenges and opportunities for CAD. IEEE/ACM international conference on computer aided design, Nov 2002, pp 203–206
5. Borkar S, Karnik T, Narendra S, Tschanz J, Keshavarzi A, De V (2003) Parameter variations and impact on circuits and microarchitecture. Proceedings of design automation conference, June 2003, pp 338–342
6. International Technology Roadmap for Semiconductors (2011) http://public.itrs.net
7. Overclockers.com website, overclockers forum (2011) http://www.overclockers.com
8. Meehan MD, Purviance J (1993) Yield and reliability in microwave circuit and system design. Artech House, Boston
9. Strojwas AJ (2006) Conquering process variability: a key enabler for profitable manufacturing in advanced technology nodes. IEEE international symposium on semiconductor manufacturing, Sep. 2006, pp xxiii–xxxii
10. Pang L-T, Qian K, Spanos CJ, Nikolic B (2009) Measurement and analysis of variability in 45 nm strained-Si CMOS technology. IEEE J Solid State Circuits 44(8):2233–2243
11. Austin T, Bertacco V, Blaauw D, Mudge T (2005) Opportunities and challenges for better than worst-case design. Proceedings of the Asia and South Pacific design automation conference, Jan 2005, pp I/2–I/7
12. Sheng W, Emira A, Sanchez-Sinencio E (2006) CMOS RF receiver system design: a systematic approach. IEEE Trans Circuits Syst-I: Reg Pap 53(5):1023–1034
13. Baltus P (2004) Minimum power design of RF front ends. PhD Dissertation, Eindhoven University of Technology
14. El-Nozahi M, Sanchez-Sinencio E, Entesari K (2009) Power-aware multiband–multistandard CMOS receiver system-level budgeting. IEEE Trans Circuits Syst II: Exp Brief 56 (7):570–574
15. Part 15.3: wireless medium access control (MAC) and physical layer (PHY) specifications for high rate wireless personal area networks (WPANs): amendment 2: millimeter-wave based alternative physical layer extension. IEEE 802.15.3c, Oct 2009
16. Janssen E, Mahmoudi R, van der Heijden E, Sakian P, de Graauw A, Pijper R, van Roermund A (2010) Fully balanced 60 GHz LNA with 37% bandwidth, 3.8 dB NF, 10 dB gain and

constant group delay over 6 GHz bandwidth. 10th topical meeting on silicon monolithic integrated circuits in RF systems, Jan 2010
17. Sakian P, Mahmoudi R, van der Heijden E, de Graauw A, van Roermund A (2011) Wideband cancellation of second order intermodulation distortions in a 60 GHz zero-IF mixer. 11th topical meeting on silicon monolithic integrated circuits in RF systems, Jan 2011
18. Tomkins A, Aroca RA, Yamamoto T, Nicolson ST, Doi Y, Voinigescu SP (2009) A zero-IF 60 GHz 65 nm CMOS transceiver with direct BPSK modulation demonstrating up to 6 Gb/s data rate over a 2 m wireless link. IEEE J Solid State Circuits 44(8):2085–2099
19. Marcu C, Chowdhury D, Thakkar C, Park J-D, Kong L-K, Tabesh M, Wang Y, Afshar B, Gupta A, Arbabian A, Gambini S, Zamani R, Alon E, Niknejad AM (2009) A 90 nm CMOS low-power 60 GHz transceiver with integrated baseband circuitry. IEEE J Solid State Circuits 44(12):3434–3447
20. Alpman E, Lakdawala H, Carley LR, Soumyanath K (2009) A 1.1 V 50 mW 2.5 GS/s 7b time-interleaved C-2C SAR ADC in 45 nm LP digital CMOS. IEEE international solid state circuits conference, Feb 2009
21. Deng W, Mahmoudi R, Harpe P, van Roermund A (2008) An alternative design flow for receiver optimization through a trade-off between RF and ADC. IEEE radio wireless symposium, Jan 2008
22. Yang J, Lin Naing T, Brodersen RW (2010) A 1 GS/s 6 Bit 6.7 mW successive approximation ADC using asynchronous processing. IEEE J Solid State Circuits 45(8):1469–1478
23. Ashby KB, Koullias IA, Finley WC, Bastek JJ, Moinian S (1996) High Q inductors for wireless applications in a complementary silicon bipolar process. IEEE J Solid State Circuits 31(1):4–9
24. Yang R, Qian H, Li J, Xu Q, Hai C, Han Z (2006) SOI technology for radio-frequency integrated-circuit applications. IEEE Trans Electron Dev 53(6):1310–1316
25. Chang JY-C, Abidi AA, Gaitan M (1993) Large suspended inductors on silicon and their use in a 2-μm CMOS RF amplifier. IEEE Electron Dev Lett 14(5):246–248
26. Yue CP, Wong SS (1998) On-chip spiral inductors with patterned ground shields for Si-based RF ICs. IEEE J Solid-State Circuits 33(5):743–752
27. Yue CP, Ryu C, Lau J, Lee TH, Wong SS (1996) A physical model for planar spiral inductors on silicon. International electron devices meeting, Dec 1996, pp 155–158
28. Weisshaar A, Lan H, Luoh A (2002) Accurate closed-form expressions for the frequency-dependent line parameters of on-chip interconnects on lossy silicon substrate. IEEE Trans Adv Pack 25(2):288–296
29. Wiemer L, Jansen RH (1987) Determination of coupling capacitance of underpasses, air bridges and crossings in MICs and MMICs. Electron Lett 23(7):344–346
30. Cheung TSD, Long JR (2006) Shielded passive devices for silicon-based monolithic microwave and millimeter-wave integrated circuits. IEEE J Solid-State Circuits 41(5):1183–1200
31. Noise figure measurement accuracy- the Y-factor method (2010), Agilent application note 57-2. http://cp.literature.agilent.com/litweb/pdf/5952-3706E.pdf
32. Pozar DM (2005) Microwave engineering. Wiley, Hoboken
33. Tiemeijer LF, Pijper RMT, van der Heijden E (2010) Complete on-wafer noise-figure characterization of 60-GHz differential amplifiers. IEEE Trans Microw Theory Tech 58(6):1599–1608
34. Agilent PSA series spectrum analyzers phase noise measurement personality (2005), technical overview with self-guided demonstration: option 226. http://cp.literature.agilent.com/litweb/pdf/5988-3698EN.pdf
35. Agilent's phase noise measurement solutions: finding the best fit for your test requirements, Selection Guide (2011). http://cp.literature.agilent.com/litweb/pdf/5990-5729EN.pdf
36. Agilent E5052A signal source analyzer: advanced phase noise and transient measurement techniques, application note (2004). http://cp.literature.agilent.com/litweb/pdf/5989-1617EN.pdf

37. Agilent E5052B signal source analyzer: advanced phase noise and transient measurement techniques, application note (2007). http://cp.literature.agilent.com/litweb/pdf/5989-7273EN.pdf
38. Walls WF (2001) Practical problems involving phase noise measurements. 33rd annual precise time and time interval meeting, Nov 2001, pp 407–416
39. Lee TH (2004) The design of CMOS radio-frequency integrated circuits. Cambridge University Press, Cambridge
40. Shaeffer DK, Lee TH (1997) A 1.5-V, 1.5-GHz CMOS low noise amplifier. IEEE J Solid-State Circuits 32(5):745–759
41. Yao T, Gordon MQ, Tang KKW, Yau KHK, Yang M-T, Schvan P, Voinigescu SP (2007) Algorithmic design of CMOS LNAs and PAs for 60-GHz radio. IEEE J Solid-State Circuits 42(5):1044–1057
42. Zhuo W, Embabi S, Pineda de Gyvez J, Sanchez-Sinencio E (2000) Using capacitive cross-coupling technique in RF low noise amplifiers and down-conversion mixer design. Proceedings of European solid state circuits conference, Sep. 2000, pp 116–119
43. Bruccoleri F, Klumperink EAM, Nauta B (2001) Generating all 2-MOS transistors amplifiers leads to new wide-band LNAs. IEEE J Solid-State Circuits 36(7):1032–1040
44. Bruccoleri F, Klumperink EAM, Nauta B (2004) Wide-band CMOS low-noise amplifier exploiting thermal noise canceling. IEEE J Solid-State Circuits 39(2):275–282
45. Cassan DJ, Long JR (2003) A 1-V transformer-feedback low-noise amplifier for 5-GHz wireless LAN in 0.18-μm CMOS. IEEE J Solid-State Circuits 38(3):427–435
46. Mason SJ (1954) Power gain in feedback amplifiers. Trans IRE Prof Group Circuit Theory CT-1(2):20–25
47. Gupta MS (1992) Power gain in feedback amplifiers, a classic revisited. IEEE Trans Microw Theory Tech 40(5):864–879
48. Singhakowinta A, Boothroyd AR (1964) On linear twoport amplifiers. IEEE Trans Circuit Theory CT-11(1):169
49. Cheema HM, Sakian P, Janssen E, Mahmoudi R, van Roermund A (2009) Monolithic transformers for high frequency bulk CMOS circuits. IEEE topical meeting on silicon monolithic integrated circuits in RF systems, Jan 2009
50. Cohen E, Ravid S, Ritter D (2008) An ultra low power LNA with 15 dB gain and 4.4 dB NF in 90 nm CMOS process for 60 GHz phase array radio. IEEE radio frequency integrated circuits symposium, June 2008, pp 61–64
51. Siligaris A, Mounet C, Reig B, Vincent P, Michel A (2008) CMOS SOI technology for WPAN. Application to 60 GHz LNA. IEEE international conference on integrated circuit design and technology and tutorial, June 2008
52. Borremans J, Raczkowski K, Wambacq P (2009) A digitally controlled compact 57-to-66 GHz front-end in 45 nm digital CMOS. IEEE international solid-state circuits conference – digest of technical papers, Feb 2009, pp 492–493
53. Weyers C, Mayr P, Kunze JW, Langmann U (2008) A 22.3 dB voltage gain 6.1 dB NF 60 GHz LNA in 65 nm CMOS with differential output. IEEE international solid-state circuits conference – digest of technical papers, Feb 2008, pp 192–606
54. Razavi B (1997) Design considerations for direct-conversion receivers. IEEE Trans Circuits Syst II: Analog Digit Signal Process 44(6):428–435
55. Gilbert B (1968) A precise four-quadrant multiplier with subnanosecond response. IEEE J Solid-State Circuits 3(4):365–373
56. Darabi H, Abidi AA (2000) Noise in RF-CMOS mixers: a simple physical model. IEEE J Solid-State Circuits 35(1):15–25
57. Lee S-G, Choi J-K (2000) Current-reuse bleeding mixer. Electron Lett 36(8):696–697
58. Vitali S, Franchi E, Gnudi A (2007) RF I/Q downconverter with gain/phase calibration. IEEE Trans Circuits Syst II: Exp Briefs 54(4):367–371
59. Razavi B (2006) A 60-GHz CMOS receiver front-end. IEEE J Solid-State Circuits 41 (1):17–22

60. Razavi B (1997) A 900-MHz CMOS direct conversion receiver. Symposium on VLSI circuits digest of technical papers, June 1997, pp 113–114
61. Heydari P (2004) High-frequency noise in RF active CMOS mixers. Proceedings of the Asia and South Pacific design automation conference, Jan 2004, pp 57–61
62. Cheng W, Annema AJ, Croon JA, Nauta B (2011) Noise and nonlinearity modeling of active mixers for fast and accurate estimation. IEEE Trans Circuits Syst I: Reg Pap 58(2):276–289
63. Weiner DD, Spina JE (1980) Sinusoidal analysis and modeling of weakly nonlinear circuits. Van Norstrand Reinhold, New York
64. Wambacq P, Sansen W (1998) Distortion analysis of analog integrated circuits. Kluwer, Boston
65. Terrovitis MT, Meyer RG (2000) Intermodulation distortion in current-commutating CMOS mixers. IEEE J Solid State Circuits 35(10):1461–1473
66. Manstretta D, Brandolini M, Svelto F (2003) Second-order intermodulation mechanisms in CMOS downconverters. IEEE J Solid State Circuits 38(3):394–406
67. Dufrene K, Boos Z, Weigel R (2007) A 0.13μm 1.5V CMOS I/Q downconverter with digital adaptive IIP2 calibration. IEEE international solid-state circuits conference digest of technical papers, Feb 2007, pp 86–589
68. Wang J, Wong AKK (2011) Effects of mismatch on CMOS double-balanced mixers: a theoretical analysis. 2001 IEEE Hong Kong electron devices meeting, Hong Kong, 2001
69. Zhang F, Skafidas E, Shieh W (2007) A 60-GHz double-balanced Gilbert cell down-conversion mixer on 130-nm CMOS. IEEE radio frequency integrated circuits symposium, Honolulu, June 2007
70. Parsa A, Razavi B (2009) A new transceiver architecture for the 60-GHz band. IEEE J Solid-State Circuits 44(3):751–762
71. Rofougaran A, Rael J, Rofougaran M, Abidi A (1996) A 900 MHz CMOS LC oscillator with quadrature outputs. IEEE international solid-state circuits conference digest of technical papers, Feb 1996, pp 392–393
72. Laskin E, Rylyakov A (2009) A 136-GHz dynamic divider in SiGe technology. IEEE topical meeting on silicon monolithic integrated circuits in RF systems, Jan 2009
73. Ng AWL, Luong HC (2007) A 1-V 17-GHz 5-mW CMOS quadrature VCO based on transformer coupling. IEEE J Solid-State Circuits 42(9):1933–1941
74. Cheema HM, Mahmoudi R, van Roermund A (2010) On the importance of chip-level EM-simulations for 60-GHz CMOS circuits. European microwave integrated circuits conference, Sep. 2010, pp 246–249
75. Cheema HM (2010) Flexible phase-locked loops and millimeter wave PLL components for 60-GHz wireless networks in CMOS. PhD Dissertation, Eindhoven University of Technology
76. Baghdady EJ, Lincoln RN, Nelin BD (1965) Short-term frequency stability: characterization, theory, and measurement. Proc IEEE 53(7):704–722
77. Cutler LS, Searle CL (1966) Some aspects of the theory and measurement of frequency fluctuations in frequency standards. Proc IEEE 54(2):136–154
78. Leeson DB (1966) A simple model of feedback oscillator noise spectrum. Proc IEEE 54 (2):329–330
79. Rael JJ, Abidi AA (2000) Physical processes of phase noise in differential LC oscillators. Proceedings of the IEEE custom integrated circuits conference, 2000, pp 569–572
80. Hajimiri A, Lee TH (1998) A general theory of phase noise in electrical oscillators. IEEE J Solid-State Circuits 33(2):179–194
81. Hajimiri A, Lee TH (1998) Corrections to "A general theory of phase noise in electrical oscillators". IEEE J Solid-State Circuits 33(6):928
82. Andreani P, Xiaoyan W, Vandi L, Fard A (2005) A study of phase noise in colpitts and LC-tank CMOS oscillators. IEEE J Solid-State Circuits 40(5):1107–1118
83. Andreani P, Fard A (2006) More on the $1/f^2$ phase noise performance of CMOS differential-pair LC-tank oscillators. IEEE J Solid-State Circuits 41(12):2703–2712
84. Fard A, Andreani P (2007) An analysis of $1/f^2$ phase noise in bipolar colpitts oscillators (with a digression on bipolar differential-pair LC oscillators). IEEE J Solid-State Circuits 42 (2):374–384

85. Mazzanti A, Andreani P (2008) Class-C harmonic CMOS VCOs, with a general result on phase noise. IEEE J Solid-State Circuits 43(12):2716–2729
86. Murphy D, Rael JJ, Abidi AA (2010) Phase noise in LC oscillators: a phasor-based analysis of a general result and of loaded Q. IEEE Trans Circuits Syst I: Reg Pap 57(6):1187–1203
87. Kim DD, Kim J, Plouchart JO, Cho C, Li W, Lim D, Trzcinski R, Kumar M, Norris C, Ahlgren D (2007) A 70 GHz manufacturable complementary LC-VCO with 6.14 GHz tuning range in 65 nm SOI CMOS. IEEE international solid-state circuits conference digest of technical papers, Feb 2007, pp 540–541
88. Huang D, Hant W, Wang N-Y, Ku TW, Gu Q, Wong R, Chang MC-F (2006) A 60 GHz CMOS VCO using on-chip resonator with embedded artificial dielectric for side, loss and noise reduction. IEEE international solid-state circuits conference digest of technical papers, Feb 2006, pp 314–315
89. Parvais B, Scheir K, Vidojkovic V, Vandebriel R, Vandersteen G, Soens C, Wambacq P (2010) A 40 nm LP CMOS PLL for high-speed mm-wave communication. 2010 Proceedings of the 36th European solid-state circuits conference, Sep. 2010
90. Bozzola S, Guermandi D, Mazzanti A, Svelto F (2008) An 11.5% frequency tuning, -184dBc/Hz noise FOM 54 GHz VCO. IEEE radio frequency integrated circuits symposium, June 2008, pp 657–660
91. Musa A, Murakami R, Sato T, Chiavipas W, Okada K, Matsuzawa A (2010) A 58-63.6GHz quadrature PLL frequency synthesizer in 65nm CMOS. 2010 IEEE Asian solid state circuits conference, Nov 2010
92. Notten MGM, Veenstra H (2008) 60GHz quadrature signal generation with a single phase VCO and polyphase filter in a 0.25μm SiGe BiCMOS technology. IEEE bipolar/BiCMOS circuits and technology meeting, Oct 2008, pp 178–181
93. Ellinger F, Morf T, Buren GV, Kromer C, Sialm G, Rodoni L, Schmatz M, Jackel H (2004) 60GHz VCO with wideband tuning range fabricated on VLSI SOI CMOS technology. IEEE MTT-S international microwave symposium digest of technical papers, vol 3, pp 1329–1332
94. Sivonen P, Vilander A, Parssinen A (2005) Cancellation of second-order intermodulation distortion and enhancement of IIP2 in common-source and common-emitter RF transconductors. IEEE Trans Circuits Syst I: Reg Pap 52(2):305–317
95. Bautista EE, Bastani B, Heck J (2000) A high IIP2 downconversion mixer using dynamic matching. IEEE J Solid-State Circuits 35(12):1934–1941
96. Chen M, Wu Y, Chang MF (2006) Active 2nd-order intermodulation calibration for direct-conversion receivers. IEEE international solid-state circuits conference digest of technical papers, Feb 2006, pp 1830–1839
97. Dufrene K, Weigel R (2006) A novel IP2 calibration method for low-voltage downconversion mixers. IEEE radio frequency integrated circuits symposium, June 2006
98. Kivekas K, Parssinen A, Ryynanen J, Jussila J, Halonen K (2002) Calibration techniques of active BiCMOS mixers. IEEE J Solid State Circuits 37(6):766–769
99. Hotti M, Ryynanen J, Kievekas K, Halonen K (2004) An IIP2 calibration technique for direct conversion receivers. IEEE international symposium on circuits and systems, May 2004
100. Ler C-L, bin A'ain AK, Kordesch AV (2008) Compact, high-Q, and low-current dissipation CMOS differential active inductor. IEEE Microw Wirel Compon Lett 18(10):683–685
101. Verbruggen B, Craninckx J, Kuijk M, Wambacq P, Van der Plas G (2010) A 2.6mW 6b 2.2GS/s 4-times interleaved fully dynamic pipelined ADC in 40nm digital CMOS. IEEE international solid-state circuits conference digest of technical papers, Feb 2010, pp 296–298
102. Lont M, Mahmoudi R, van der Heijden E, de Graauw A, Sakian P, Baltus P, van Roermund A (2009) A 60GHz Miller effect based VCO in 65nm CMOS with 10.5% tuning range. IEEE topical meeting on silicon monolithic integrated circuits in RF systems, 19–21 Jan 2009
103. Stadius K, Kaumisto R, Porra V (1999) Varactor diodeless harmonic VCOs for GHz-range applications. ICECS 1:505–508